LA-UR-15-20435
Approved for public release; distribution is unlimited.

Title: Anisotropic Elastic-Waveform Modeling for Fracture Characterization in EGS Reservoirs

Author(s): Gao, Kai
Huang, Lianjie

Intended for: Proceedings of Fourtieth Workshop on Geothermal Reservoir Engineering

Issued: 2015-01-26

PROCEEDINGS, Fourtieth Workshop on Geothermal Reservoir Engineering
Stanford University, Stanford, California, January 26-28, 2015
SGP-TR-204

Anisotropic Elastic-Waveform Modeling for Fracture Characterization in EGS Reservoirs

Kai Gao and Lianjie Huang

kaigao@lanl.gov, ljh@lanl.gov

Los Alamos National Laboratory, Los Alamos, NM 87545, U.S.A.

Keywords: anisotropy, elastic, fracture characterization, optimized finite-difference method, staggered-grid, rotated coordinates.

ABSTRACT

Enhanced geothermal systems (EGS) contain newly created fractures in addition to possible existing fractures. Accurate characterization and monitoring of EGS reservoirs are crucial for optimal placement of new wells and effective extraction of geothermal heat. The fractured reservoirs behave as anisotropic media where seismic waves propagate with different velocities along different directions. In addition, the anisotropic properties of fluid-filled fracture zones could be different from those of dry fracture zones. We develop an optimized rotated staggered-grid elastic-wave finite-difference method for simulating seismic-wave propagation in heterogeneous, anisotropic media. Our new method uses a few extra grid points and optimized finite-difference coefficients based on the space-time dispersion relation, and reduce numerical dispersion of the conventional rotated staggered-grid finite-difference scheme. We validate our new method using synthetic vertical-seismic-profiling (VSP) data for an anisotropic geophysical model built with geologic features found at the Raft River EGS reservoir. This improved and optimized rotated staggered-grid finite-difference method provides an essential tool for analyzing VSP data, reverse-time migration, and elastic-waveform inversion in anisotropic, fractured reservoirs.

1. INTRODUCTION

The elastic-waveform inversion (EWI) is becoming a powerful tool for accurately characterizing complex geological structures using multi-component seismic data. EWI is to infer subsurface structures and medium properties by minimizing the difference between the recorded data and synthetic data. Most current waveform inversion algorithms assume acoustic media or isotropic elastic media and are implemented either in the time domain or in the frequency domain (e.g., Tarantola, 1984; Virieux and Operto, 2009; Guitton, 2012; Lin and Huang, 2015). EGS usually contains fractures that preferentially align along one or more spatial directions, making the reservoir anisotropic. Therefore, anisotropic elastic-waveform inversion is needed for fracture characterization in EGS reservoirs.

A fundamental tool in developing EWI for anisotropic media is the fast yet accurate solver to simulate elastic wavefield propagation in anisotropic media. There have been many attempts, such as finite-difference method (e.g., Virieux, 1986), the spectral-element method (Komatitsch and Tromp, 1999) and discontinuous Galerkin (DG) method (Dumbser and Kaser, 2006) to solve the elastic wave equation. The conventional staggered-grid (SG) finite-difference method (Virieux, 1986) is the most popular scheme among these methods because of its simplicity and accuracy. Although the conventional SG scheme can properly handle anisotropy such as transverse isotropy with vertical symmetry axis (VTI) or horizontal symmetry axis (HTI), and orthohombic anisotropy, the method requires to interpolate wavefield velocity components for other more complicated anisotropic media, such as media containing transverse isotropy with a tilted symmetry axis (TTI), monoclinic anisotropy, or triclinic anisotropy. Wavefield interpolation could lead to inaccurate simulation of seismic-wave propagation in anisotropic media. In addition, since the stress components are not all defined at the same grid points in the SG scheme, it is necessary to interpolate some of elastic parameters on the grid points of shear stress components even in the isotropic case or VTI/HTI case, resulting in additional numerical errors.

Saenger et al. (2000) proposed the so-called rotated staggered-grid finite-difference stencil (RSG) to avoid these problems, where the stress components and all the elasticity parameters are defined on the same grid points, and velocity components and density are defined at the same grid points. The RSG is known to have larger numerical dispersion compared with SG using the same temporal and spatial discretization (Saenger and Bohlen, 2004). Several optimized finite-difference methods were developed based on either the spatial dispersion relation or temporal-spatial dispersion relation of the wave equation to reduce the numerical dispersion during modeling (e.g., Liu, 2013; Tan and Huang, 2014).

We develop an optimized RSG finite difference method for modeling elastic-wave propagation in anisotropic media. We employ a finite-difference stencil along the rotated coordinates similar to the stencil used by Tan and Huang (2014) in the regular coordinates. That is, our optimized rotated-staggered grid (ORSG) stencil uses some extra points off the rotated coordinates and employs the optimized coefficients calculated based on minimizing the space-time dispersion relation. The resulting ORSG finite-difference stencil contains more grid points compared with the conventional RSG. However, we demonstrate using dispersion curves that the ORSG can indeed achieve a higher computational efficiency compared to the conventional RSG scheme. We use our new method to conduct numerical modeling of VSP wavefields in an anisotropic geophysical model built using geologic features at the Raft River EGS field (Ayling and Moore, 2013), and compare the wavefields with those computed using an isotropic model.

Our paper is organized as follows. We first introduce our ORSG finite-difference stencil, and compare the dispersion curve of our ORSG method with that of the conventional RSG scheme. We then show a numerical example to demonstrate the importance of simulating anisotropic wave propagation in EGS reservoirs for reliable imaging and waveform inversion for fracture characterization.

2. METHODOLOGY

We introduce the methodology of our optimized rotated staggered-grid finite-difference method for modeling elastic-wave propagation in anisotropic media.

2.1 Elastic-wave equation modeling in anisotropic media

2.1.1 Elastic-wave equation

The elastic-wave equation in the stress-velocity formulation (Carcione, 2007) is given by

$$\frac{\partial \boldsymbol{\sigma}}{\partial t} = \mathbf{c} : \boldsymbol{\varepsilon}, \qquad \rho \frac{\partial \mathbf{v}}{\partial t} = \nabla \cdot \boldsymbol{\sigma}, \tag{1}$$

where $\boldsymbol{\sigma} = (\sigma_{11}, \sigma_{33}, \sigma_{13})$ is the stress wavefield, $\mathbf{v} = (v_1, v_3)$ is the particle velocity wavefield, $\boldsymbol{\varepsilon} = [\nabla \mathbf{v} + (\nabla \mathbf{v})^{\mathrm{T}}]/2$ is the strain wavefield, ρ is the mass density and $\mathbf{c} = c_{ijkl}$ is the elasticity tensor that can be written in a matrix C_{IJ} with the Voigt notation for 2-D elastic media as

$$\mathbf{C} = \begin{pmatrix} C_{11} & C_{13} & C_{15} \\ C_{13} & C_{33} & C_{35} \\ C_{15} & C_{35} & C_{55} \end{pmatrix}. \tag{2}$$

This elasticity matrix describes the anisotropy up to monoclinic anisotropy and transverse isotropy with tilted axis (TTI), with the x_1x_3 plane as the symmetry plane.

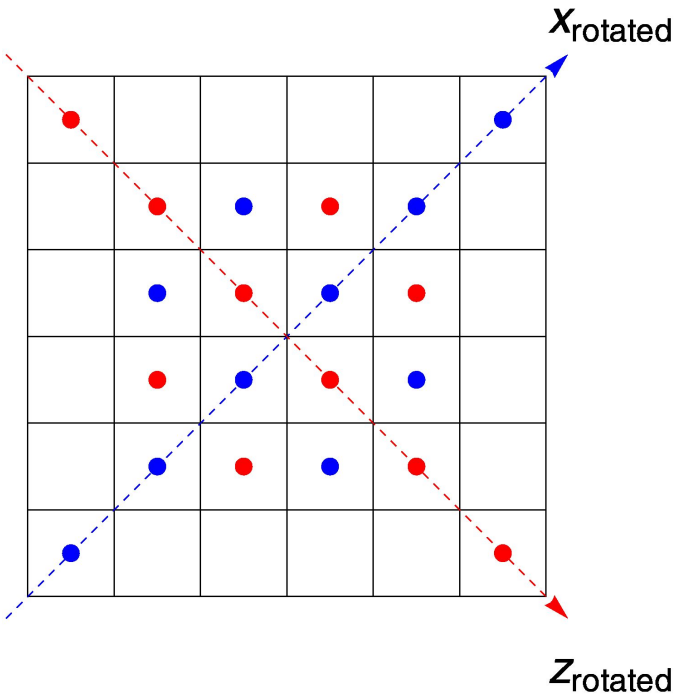

Figure 1: Finite-difference stencil for our ORSG finite-difference method: blue and red axis represents the rotated *x*- and *z*-axis, respectively, and blue and red dots represent the grid points used to calculate the staggered finite-difference approximation of the first-order derivatives along the two rotated axes, respectively. Note there are four off-axis points for each rotated axis in our ORSG scheme.

2.1.2 Optimized Rotated Staggered-Grid Finite-Difference Scheme

Figure 1 shows the fundamental difference between the conventional RSG and our ORSG. The conventional RSG stencil uses the blue or red grid points along each rerated coordinate, while our ORSG stencil employs four extra points for each rotated axis. This idea is inspired by the work of Tan and Huang (2014) for constructing optimized SG for acoustic-wave modeling. Our ORSG finite-difference

stencils have 4th order accuracy in time and 2*L*-th order spatial accuracy for the first-order partial derivatives along two rotated axes, i.e., $\partial / \partial \tilde{x}$ and $\partial / \partial \tilde{z}$, at the point (i, j) as

$$\frac{\partial f}{\partial \tilde{x}} = \frac{1}{\Delta r}\left\{\sum_{m=1}^{L} c_m \left[f(i+m^-, j-m^-) - f(i-m^-, j+m^-) \right] + d_0 \left[f\left(i-\frac{1}{2}, j-\frac{3}{2}\right) - f\left(i-\frac{3}{2}, j-\frac{1}{2}\right) + f\left(i+\frac{3}{2}, j+\frac{1}{2}\right) - f\left(i+\frac{1}{2}, j+\frac{3}{2}\right) \right] \right\}, \tag{3}$$

$$\frac{\partial f}{\partial \tilde{z}} = \frac{1}{\Delta r}\left\{\sum_{m=1}^{L} c_m \left[f(i+m^-, j+m^-) - f(i-m^-, j-m^-) \right] + d_0 \left[f\left(i+\frac{3}{2}, j-\frac{1}{2}\right) - f\left(i+\frac{1}{2}, j-\frac{3}{2}\right) + f\left(i-\frac{1}{2}, j+\frac{3}{2}\right) - f\left(i-\frac{3}{2}, j+\frac{1}{2}\right) \right] \right\}, \tag{4}$$

where $m^- = m - 1/2$, c_m $(m = 1, \cdots, L)$ are the coefficients for the points along the rotated axes, d_0 is the coefficient for the points off the rotated axes, and $\Delta r = \sqrt{\Delta x^2 + \Delta z^2}$ computed using the grid intervals Δx and Δz along the regular coordinates. In contrast to the conventional finite-difference coefficients based on the Taylor expansion that have analytical expressions, the optimized finite-difference coefficients are functions of the dispersion parameter $r = v\Delta t / \Delta h$, where Δt is the time interval in the modeling, and Δh is the grid size for the modeling. We adopt the coefficients in Tan and Huang (2014) with an enlarged grid spacing, i.e., $\sqrt{2}$ times of the grid spacing on the regular coordinates when $\Delta x = \Delta z$, to obtain the optimized coefficients for our ORSG.

Because seismic waves may propagate with different speeds along different directions in anisotropic media, we first solve the Christoffel equation (Carcione, 2007) to compute the phase velocities of the qSV-wave along 360 directions with a one-degree interval, then we choose the minimum phase velocity to calculate the dispersion parameter r, and compute the optimized finite-difference coefficients using this r value. A high-order ORSG stencil with 16th order accuracy in space involves 16 points along each rotated axis and 4 points off each rotated axis. Therefore, the calculation of first-order derivative for each grid point in our ORSG uses a total of 40 grid points, while the conventional RSG uses only 32 grid points. On the other hand, ORSG allows us to use a time interval larger than that for RSG. In combination, our new ORSG not only is more accurate but also is computationally more efficient than RSG.

2.1.2 Comparison of numerical dispersions between ORSG and RSG

We compare numerical dispersion of our new ORSG with that of the conventional RSG. Similar to the analysis in Tan and Huang (2014), we write the relative phase velocity error in RSG as

$$e = \frac{1}{rk\Delta h} \arccos[1 - 2(g_1^2 + g_3^2) r^2] - 1, \tag{5}$$

where

$$g_1 = \sum_{m=1}^{L} c_m \sin[(m - \frac{1}{2}) k_x \Delta h] \cos[(m - \frac{1}{2}) k_z \Delta h], \tag{6}$$

$$g_3 = \sum_{m=1}^{L} c_m \cos[(m - \frac{1}{2}) k_x \Delta h] \sin[(m - \frac{1}{2}) k_z \Delta h], \tag{7}$$

and k is the wavenumber, k_x and k_z are the x_1- and x_3-component of k, respectively, c_m are the conventional staggered-grid finite-difference coefficients obtained using the Taylor expansion.

The relative phase velocity error in our ORSG is given by

$$e = \frac{1}{rk\Delta h} \arccos[1 - 2(h_1^2 + h_3^2) r^2] - 1, \tag{8}$$

where

$$h_1 = \sum_{m=1}^{L} c_m \sin[(m - \frac{1}{2}) k_x \Delta h] \cos[(m - \frac{1}{2}) k_z \Delta h] + 2d_0 \cos(\frac{1}{2} k_z \Delta h) \sin(\frac{1}{2} k_x \Delta h)[1 + \cos(k_x \Delta h) - \cos(k_z \Delta h)], \tag{9}$$

$$h_3 = \sum_{m=1}^{L} c_m \cos[(m - \frac{1}{2}) k_x \Delta h] \sin[(m - \frac{1}{2}) k_z \Delta h] + 2d_0 \cos(\frac{1}{2} k_x \Delta h) \sin(\frac{1}{2} k_z \Delta h)[1 + \cos(k_z \Delta h) - \cos(k_x \Delta h)], \tag{10}$$

and c_m and d_0 are the optimized finite-difference coefficients that are functions of dispersion parameter r.

We calculate the relative phase velocity errors for both RSG and ORSG when dispersion parameter $r = 0.1$. Figure 2 shows the calculated absolute values of the phase velocity errors along $\theta = 0$ direction for 16th-order RSG, 16th-order ORSG and 32nd-order RSG. The ORSG clearly has smallest dispersion at almost all the wavenumber range among the three schemes, and the error is much smaller compared with those of RSG of the same order at large wavenumbers. The 16th-order ORSG has similar dispersion with that of 32nd-order RSG at large wavenumbers. However, 32nd-order RSG involves 64 grid points to calculate the first-order spatial derivative for each grid point, while our ORSG needs only 40 grid points.

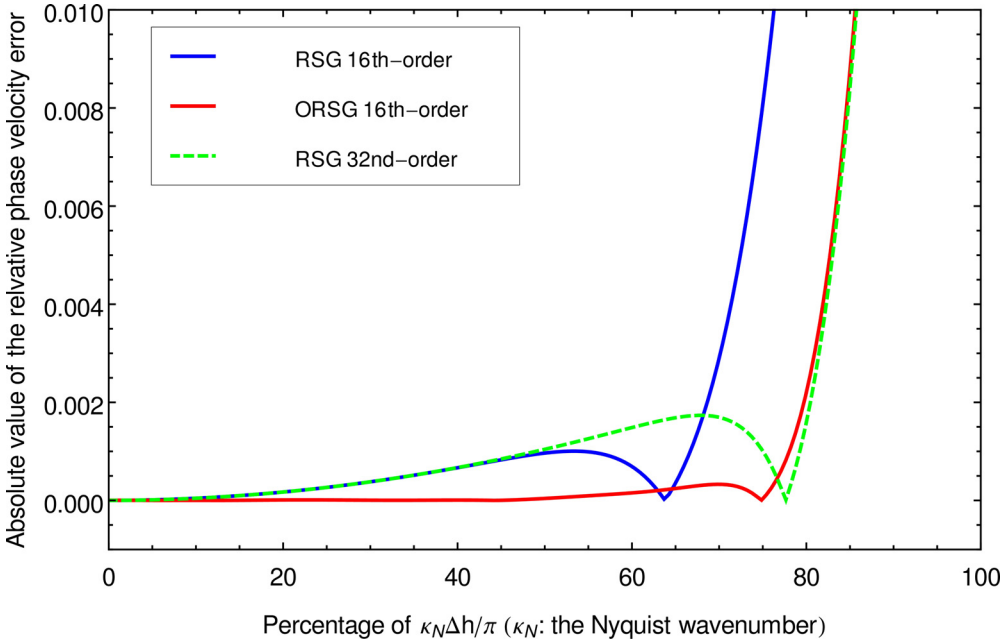

Figure 2: Dispersion curves of the conventional RSG with 16th-order accuracy in space (blue), the ORSG with 16th-order accuracy (red) and conventional RSG with 32nd-order accuracy. The propagation direction is $\theta = 0$.

3. RESULTS AND ANALYSIS

In this section, we show a numerical example with our ORSG for a geophysical model built using geologic features found at the Raft River geothermal field in Idaho (Ayling and Moore, 2013). Figure 3 displays the models of elasticity parameters C_{11}, C_{13}, C_{33} and C_{55}. We set $C_{15} = C_{35} = 0$. The model contains a vertical narrow structure. We discretize the model with a grid interval of 7 m along both horizontal and vertical directions. We assume that the vertical narrow structure contains randomly distributed vertical fractures (transverse isotropy with horizontal axis, or HTI), and let elasticity constant C_{33} be $C_{33} = 2C_{11}$. For comparison, we also conduct numerical modeling for the case when the narrow structure is an isotropic elastic medium with $C_{33} = C_{11}$.

We simulate an offset VSP dataset for the source at 70 m in depth and 875 m in the horizontal direction, and a total of 300 receivers placed in a vertical borehole penetrating the vertical narrow structure. We use a Ricker wavelet with a central frequency of 40 Hz as the source function.

Figure 4 shows simulated common-shot VSP wavefields. Figures 4(a) and (b) are the horizontal particle velocity components when assuming the vertical narrow structure is HTI anisotropic and isotropic, and Fig. 4(c) depicts their differences magnified by 10 times. Figures 4(d-f) are the corresponding vertical components of the simulated wavefields. Even though the narrow structure is quite small in size, the resulting wavefield differences caused by anisotropy within the structure are significant, as shown in Figs. 4(c) and (f). Imaging and inversion based on full wavefields, such as the anisotropic elastic full-waveform inversion, rely on these differences to infer the characteristics of the reservoir. A reliable description of the medium properties and the accurate modeling of seismic wavefields are therefore vitally important for such tasks.

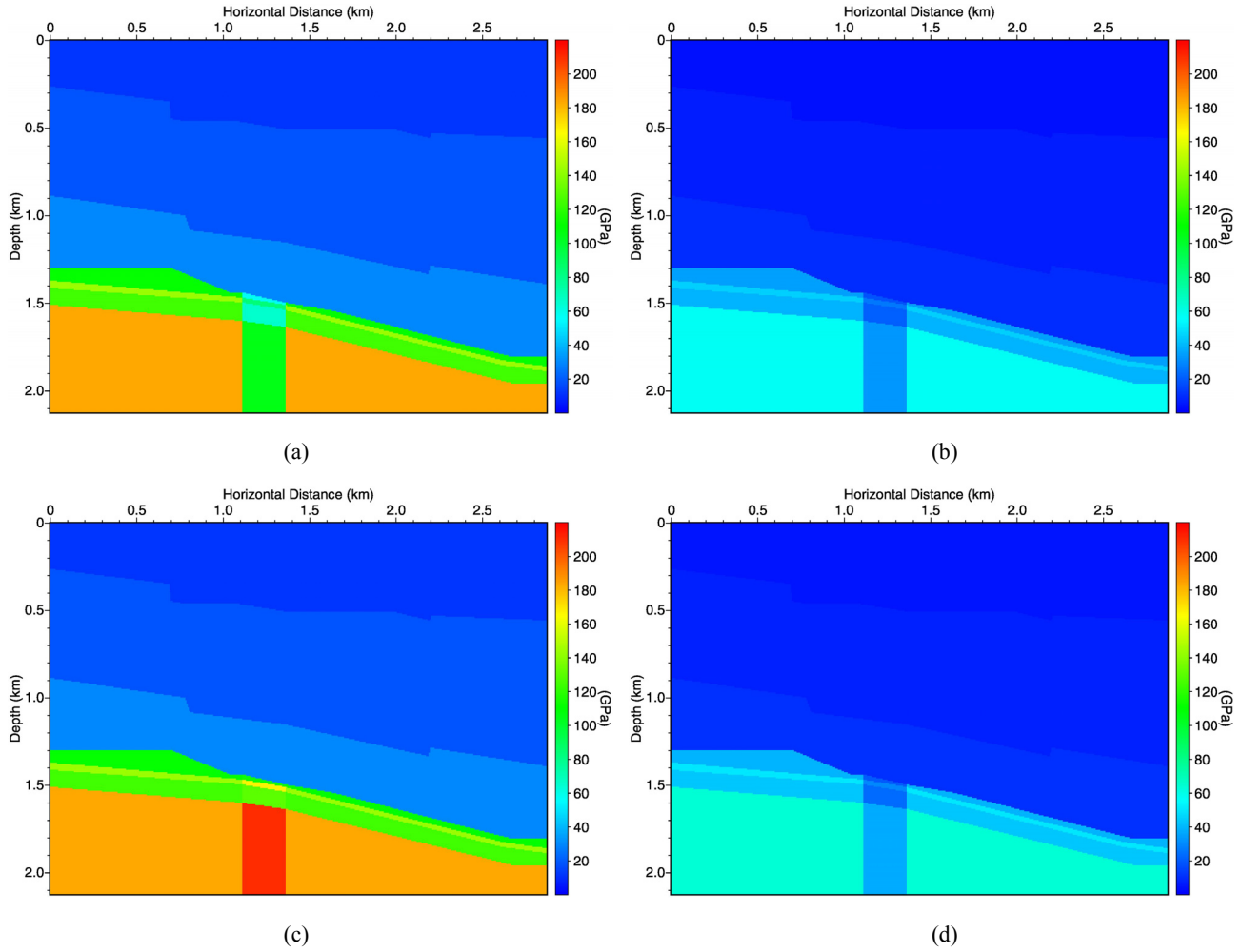

Figure 3: Elasticity parameter models for numerical wavefield modeling. (a) C_{11} model, (b) C_{13} model, (c) C_{33} model, and (d) C_{55} model. Note the difference between C_{11} and C_{33} in the vertical narrow structure.

4. CONCLUSIONS

We have developed an optimized rotated staggered-grid finite-difference method for modeling seismic-wave propagation in anisotropic elastic media. Our optimized rotated staggered-grid finite-difference stencil incorporates a few extra grid points off the rotated axes and employs finite-difference coefficients optimized in the space-time domain. This optimized finite-difference method has lower numerical dispersion compared with the conventional rotated-staggered grid finite-difference method, while preserving all the advantages of rotated staggered-grid finite difference method such as that there is no need to interpolate elasticity parameters or wavefield velocity components during numerical modeling. We have validated our new method using a geophysical model containing an anisotropic region and demonstrated the importance of accounting for anisotropy for characterizing fractured EGS reservoirs.

5. ACKNOWLEDGMENTS

This work was supported by the Geothermal Technologies Office of the U.S. Department of Energy through contract DE-AC52-06NA25396 to Los Alamos National Laboratory. The computation was performed on super-computers provided by the Institutional Computing Program of Los Alamos National Laboratory.

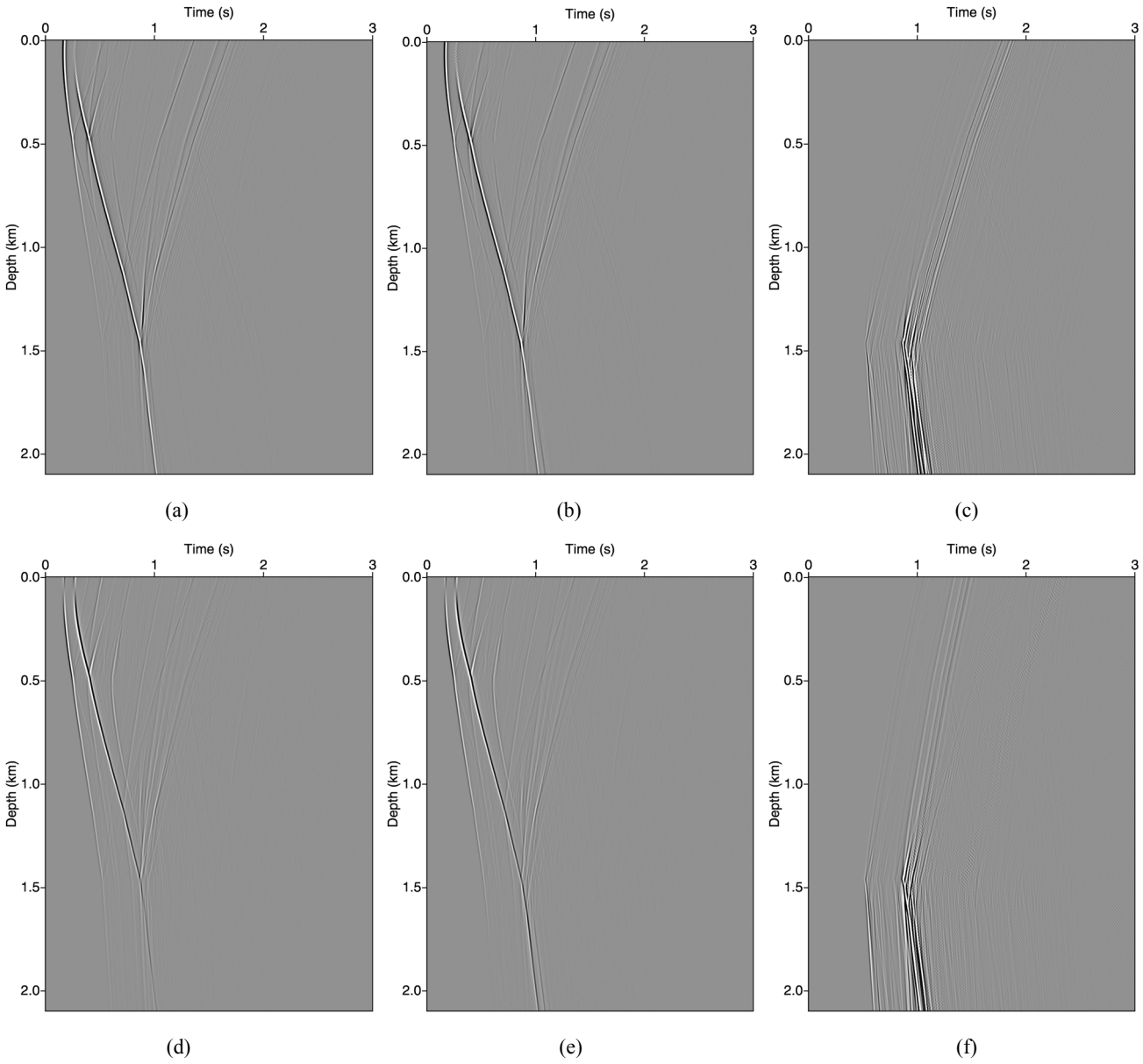

Figure 4: Horizontal (a-c) and vertical (d-f) particle velocity components of simulated offset VSP wavefields: (a) and (d) are for the case when the vertical narrow structure is HTI anisotropic, (b) and (e) are for the isotropic narrow structure , (c) shows wavefield differences between (a) and (b), and (f) displays wavefield difference between (d) and (e). Wavefield differences in (c) and (f) are magnified by a factor of 10.

REFERENCES

Ayling, B., and Moore, J.: Fluid geochemistry at the Raft River geothermal field, Idaho, USA: New data and hydrogeological implications, *Geothermics*, **47**, (2013), 116-126.

Carcione, J.: Wave Fields in Real Media: Wave Propagation in Anisotropic, Anelastic, Porous and Electromagnetic Media, 2nd edition, Elsevier Science, Amsterdam, (2007).

Dumbser, M., and Kaser, M.: An arbitrary high-order discontinuous Galerkin method for elastic waves on unstructured meshes-II. The three-dimensional isotropic case, *Geophysical Journal International*, **167**, (2006), 319–336.

Guitton, A.: Blocky regularization schemes for full waveform inversion, *Geophysical Prospecting*, **60**, (2012), 870–884.

Komatitsch, D., and Tromp, J.: Introduction to the spectral-element method for 3-D seismic wave propagation: *Geophysical Journal International*, **139**, (1999), 806–822.

Lin, Y., and Huang, L.: Acoustic- and elastic-waveform inversion using a modified total-variation regularization scheme, *Geophysical Journal International*, 200, (2015), 489-502.

Liu, Y.: Globally optimal finite-difference schemes based on least squares, *Geophysics*, **78**(4), (2013), T113-T132.

Saenger, E. H., N. Gold, and S. A. Shapiro: Modeling the propagation of elastic waves using a modified finite-difference grid, *Wave Motion*, **31**, (2000), 77–92.

Saenger, E.H., and Bohlen, T.: Finite-difference modeling of viscoelastic and anisotropic wave propagation using the rotated staggered grid, *Geophysics,* **69**(2), (2004), 583-591.

Tan, S., and Huang, L.: A staggered-grid finite-difference scheme optimized in the time–space domain for modeling scalar-wave propagation in geophysical problems, *Journal of Computational Physics*, **276**, (2014), 613-634.

Tarantola, A.: Inversion of seismic reflection data in the acoustic approximation, *Geophysics*, **49**(8), (1984), 1259–1266.

Virieux, J.: P-SV wave propagation in heterogeneous media: Velocity stress finite difference method: *Geophysics*, **51**, (1986), 889–901.

Virieux, J., and Operto, S.: An overview of full-waveform inversion in exploration geophysics, *Geophysics*, **74**(6), (2009), WCC1–WCC26.